Electric Field Manipulation of Proton Conduction Pathways in Yttrium-Doped Barium Zirconate

A. Dao, P. Chakraborty, M. A. Gomez

Department of Chemistry, Mount Holyoke College, South Hadley, MA

Abstract

Centrality provides insights into proton traps and highways in proton conducting systems[1]. Applying an electric field can manipulate these pathways by adjusting energy barriers to favor a specific conduction direction. Prior studies[1] used kinetic Monte Carlo (kMC) simulations to examine proton conduction pathways in 12.5% yttrium-doped barium zirconate ($BaZr_{0.875}Y_{0.125}O_3$). Continuation study[2] showed that protons were trapped near yttrium most of the time and occasionally found longer proton pathways aided by a small applied electric field. Building on this, energies ranging from 0.0 eV to -1.0 eV and 0.0 eV to 1.0 eV are applied to the system in the +z-direction and –z-direction, respectively. Improved centrality measures are also used to highlight how electric fields shift proton traps and highways. Results show that energy barriers in the direction of the electric field are lower while those in the opposite direction are raised. Additionally, increased field strength made several sites more prominent in centrality while others became less prominent. Comparing new centrality images with kMC trajectories under an electric field revealed some modulation of proton pathways. These findings highlight how electric fields determine the direction of proton conduction in otherwise isomorphic materials.

Introduction

Understanding and optimizing proton conduction pathways is critical for enhancing the performance of proton-conducting materials. Yttrium-doped perovskites have been identified using centrality analysis as among the most efficient conducting doped perovskites[1]. Previous studies[2] observed that the most probable proton highways occurred predominantly when protons traveled in the z-direction of the perovskites. Therefore, this study aims to investigate the effect of electric field on proton pathways by applying a potential range from -1.0 eV to 1.0 eV in the z-direction of the catalyst. Additionally, limiting barriers for each step of a chosen 8-step pathway were analyzed under the influence of these electric fields. Furthermore, flow-through centrality will be used to visualized the flow of proton binding sites, as it provide clearer visualization for studying the impact of the electric field on proton pathways. Return-flow centrality of a site i is the inverse of the mean time of the first return to i. In this context, darker centrality indicates quicker proton return to site i. Figure 2 demonstrates that flow-through centrality shows a higher concentration near the dopant compared to return-flow centrality.

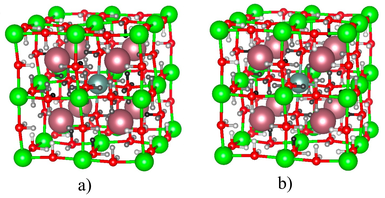

a) b)

Figure 1. a) shows the original centrality for all binding sites, where the grayscale is the function of the return flow centrality, and b) shows the flow-through centrality for all binding sites, where the grayscale is the function of how the proton flows through the sites.

References

[1] R. A. Krueger, F. G. Haibach, D. L. Fry, M. A Gomez, J. Chem. Phys. **2015** 142, 143110.
[2] M. A. Gomez, D. L. Fry, M. E. Sweet, J. of the Korean Ceramic Society. **2016** 53, 5, 521.
[3]K. S. Gomez-Haibach and M. A. Gomez, J. Phys. Chem. B **2023** 127 (43), 9258-9266
[4]R. Pornprasertsuk, J. Cheng, H. Huang, F. B. Prinz, Solid State Ionics **2007** 178(3): 195-205.
[5]M. A. Gomez, et al., J. Chem. Phys. **2021** 154, 074711
[6]Z. Lin, S. Lin, Y. Tian, A. V. Bokkelen, M. Valerio, and M. A. Gomez J. Phys. Chem. C **2020** *124* (51), 27954-27964

Results

Sites\Potential (eV)	0.00	-0.20	-0.32	-0.40	-0.60	-0.80	-1.00
$T_{IIDFar \rightarrow IIDClose}$ (1)	0.15	0.14	0.13	0.13	0.12	0.11	0.09
$R_{IIDClose \rightarrow IINDFar}$ (2)	0.04	0.03	0.02	0.02	0.01	0.00	-0.02
$R_{IINDFar \rightarrow IIDFar}$ (3)	0.06	0.05	0.04	0.04	0.03	0.02	0.00
$T_{IIDFar \rightarrow IIDClose}$ (4)	0.15	0.14	0.13	0.13	0.12	0.11	0.09
$T_{IIDClose \rightarrow IFar}$ (5)	0.04	0.03	0.02	0.02	0.01	0.00	-0.02
$R_{IFar \rightarrow IFar}$ (6)	0.02	0.01	0.00	0.00	-0.01	-0.02	-0.04
$R_{IFar \rightarrow IClose}$ (7)	0.10	0.09	0.08	0.08	0.07	0.06	0.04
$T_{IClose \rightarrow IIDFar}$ (8)	0.01	0.09	0.13	0.17	0.24	0.32	0.40

Table 1. shows the barriers for a chosen 8-steps path when potential range from 0.0 eV to -1.0 eV is applied to the system. The first column specified the type of transition, the name of sites, and the sheet number that the movement start. The greatest limiting barrier(s) for each potential applied is highlighted in orange.

Sites\Potential (eV)	0.00	0.20	0.30	0.40	0.60	0.80	1.00
$T_{IIDFar \rightarrow IClose}$ (1)	0.11	0.19	0.22	0.27	0.34	0.42	0.50
$R_{IClose \rightarrow IFar}$ (2)	0.04	0.03	0.02	0.02	0.01	0.00	-0.02
$R_{IFar \rightarrow IFar}$ (3)	0.02	0.01	0.00	0.00	-0.01	-0.02	-0.04
$T_{IFar \rightarrow IIDClose}$ (4)	0.14	0.13	0.12	0.12	0.11	0.10	0.08
$T_{IIDClose \rightarrow IIDFar}$ (5)	0.01	0.00	-0.01	-0.01	-0.02	-0.03	-0.05
$R_{IIDFar \rightarrow IINDFar}$ (6)	0.24	0.23	0.22	0.22	0.21	0.20	0.18
$R_{IINDFar \rightarrow IIDClose}$ (7)	0.00	-0.01	-0.02	-0.02	-0.03	-0.04	-0.06
$T_{IIDClose \rightarrow IIDFar}$ (8)	0.01	0.00	-0.01	-0.01	-0.02	-0.03	-0.05

Table 2. shows the barriers for a chosen 8-steps path when potential range from 0.0 eV to 1.0 eV is applied to the system. The first column specified the type of transition, the name of sites, and the sheet number that the movement start. The greatest limiting barrier(s) for each potential applied is highlighted in orange.

We observed that as the electric field strength increases, migration barriers decreases for every movement except for the transition between the first and last potential sheets. Specifically, when the potential is applied in the +z-direction, the original highest barriers of the intraoctahedral transfer (T) from H_{IID}^{Far} to H_{IID}^{Close} decreases, highlighted in orange in Table 1. A similar pattern is observed when the potential is applied in -z-direction, where the highest barriers of the rotation (R) from H_{IID}^{Far} to H_{IIND}^{Far} decreases, as shown in Table 2. When the potential applied to the system exceeds 0.30 eV in both directions, the intraoctahedral transfer (T) between H_{I}^{Close} and H_{IID}^{Far} exhibits the highest barrier. These significant barriers are marked in Figure 1 and 2 in orange and black.

When potential is applied in the positive direction, centrality of H_{IIDFar} and $H_{IIDClose}$ in the first and second potential sheets, respectively, decreases. Centrality for sites in the middle of the path, where the dopant is further away, remains consistent. Centrality of H_{IClose} in the last sheet slightly increases at V = -0.2 eV, then decreases with increasing field strength. When potential is applied in the negative direction, centrality for the site located in the last sheet increases at V = 0.2 eV, remains consistent, and slightly decreases at V = 0.8 eV, followed by another decrease at V = 1.0 eV. Centrality for the rest of the sites remains relatively consistent.

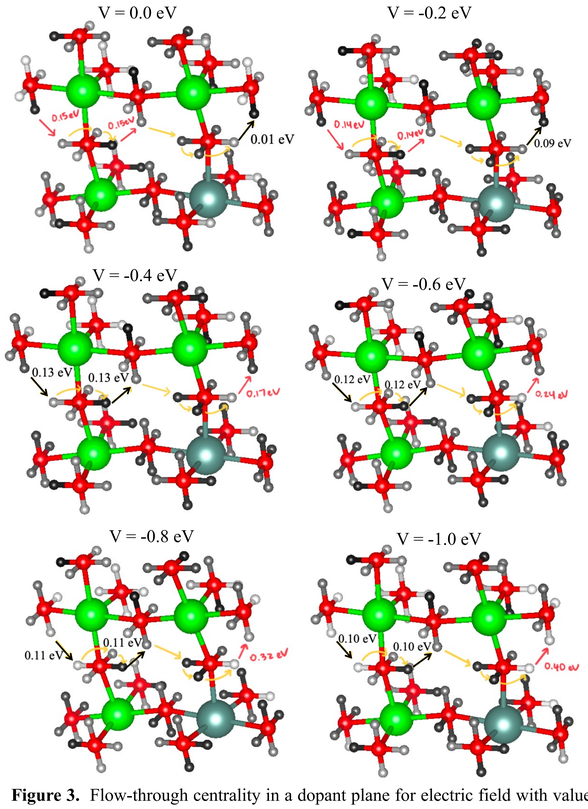

Figure 3. Flow-through centrality in a dopant plane for electric field with value 0.0 eV to -1.0 eV, applied in the –z-direction. Proton paths are shown in yellow arrow. Steps with highest limiting barriers in each path is highlighted in red. Steps can have highest limiting barriers are noted in black.

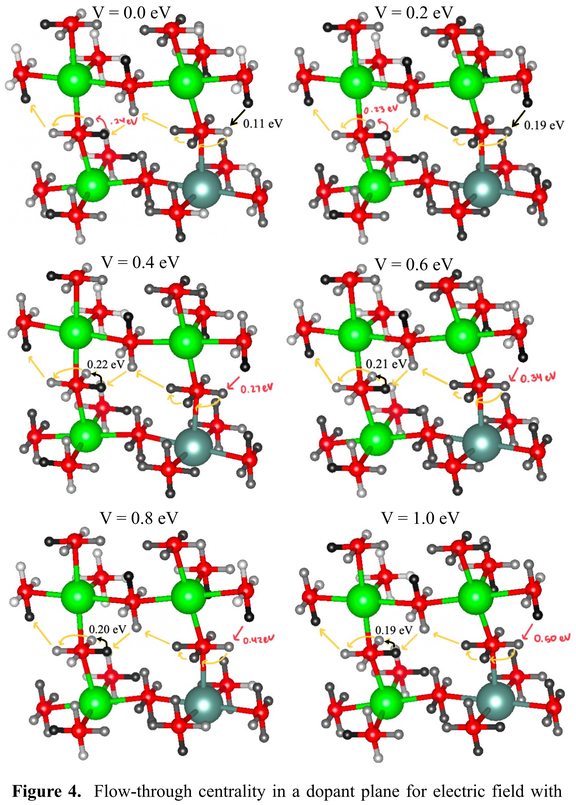

Figure 4. Flow-through centrality in a dopant plane for electric field with value 0.0 eV to 1.0 eV, applied in the –z-direction. Proton paths are shown in yellow arrow. Steps with highest limiting barriers in each path is highlighted in red. Steps can have highest limiting barriers are noted in black.

Method

A. Barrier and Electric Field

The method developed by Pornprasertsuk et al.[4] was adapted to study the impact of electric fields. The new barrier is modified as $E_{new} = E_{trans} + \alpha q V_{shift}$. Here, E_{trans} represents the original transition barrier, and α is the shape factor of the transition barriers, set to 0.5 for symmetry in this study. q denotes the charge of the proton (+1e), and V_{shift} is the potential different of the system. To simplify calculations, the perovskite was divided into 8 potential sheets, as shown in Figure 2. Each potential sheet has two components: electrode potential and space charge potential. For example, for sheet 1, $V_1 = V_{elec\,1} + V_{spc\,1}$, and so forth. According to our data set[5], there are 96 binding sites, with each site locate within one of the 8 potential sheets. To compute V_{shift} when the proton moves from site i to site j, $V_{shift\,ij} = V_{sheet\,j} - V_{sheet\,i}$. This value was then used to compute the modified barriers and rate constants from site i to site j.

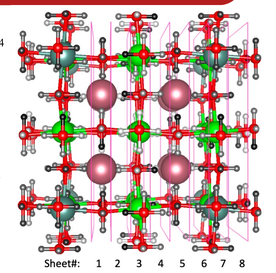

Figure 2. shows the flow-through centrality for all binding sites with 8 potential sheets

B. Centrality

From the energy dataset[5], flow-through centrality was calculated using m_{ij} - the mean time to travel from site i to site j - to visualize the flow of paths through all binding sites with the following formular:

$$C_t = \frac{1}{\frac{1}{N(N-1)}\sum_i \sum_j \frac{m_{it} + m_{tj}}{m_{ij}}}$$

When $\frac{m_{it}+m_{tj}}{m_{ij}} < 1$, the mean time to go from i to j through t is shorter, indicating more effective conduction, resulting in a higher flow-through centrality.

Conversely, when $\frac{m_{it}+m_{tj}}{m_{ij}} > 1$, the flow through t suggests ineffective conduction, resulting in a lower flow-through centrality. Flow through centrality thus is larger when on average site t speeds up conduction making the denominator smaller.

Critical to the flow through centrality calculation is the calculation of m_{ij}.

$$m_{ij} = p_{ij}\left(\frac{1}{k_{ij}}\right) + \sum_l p_{il}\left(\frac{1}{k_{il}} + m_{lj}\right)$$

The details of calculating this average are shown in reference 1.

Conclusion

While the barriers of the intraoctahedral transfer between H_{I}^{Close} in the last sheet where the full applied field is felt and H_{IID}^{Far} in the first sheet shows an irregular trend in simulation, such a transfer is not possible in a physical system which would have no periodic boundary conditions in the applied field. Consequently, in the chosen 8-step path, every possible movement that could occur in a real system benefitted from the electric field as expected. The limiting barrier type changes when the field is reversed from intraoctahedral transfer in the +z-direction to rotation in the -z-direction. The centrality of sites visited by protons in the middle of the path (farther from the dopant) remained relatively constant in both directions. However, centrality of sites located in the first and last sheets changes as the field strength increases. The system size needs to increase and the z-periodic boundary conditions need to be removed for a more realistic system.

Moving forward, our investigation will focus on further exploring proton conduction in a larger system periodic only in x and y directions as we apply an oscillating electric field to understand the types of motions that electrochemical impedance spectroscopy probes. Additionally, we plan to repeat the calculations with another energy dataset that better aligns with experimental results.

Acknowledgement

This research was supported by the National Science Foundation under grant DMR1709975 and the Mount Holyoke College Department of Chemistry. Computational resources were provided in part by the MERCURY consortium under NSF grant CHE-1626238 and 2018427.